On the Use of Nonfluorescent Dye Labeled Ligands in FRET-Based Receptor Binding Studies

Chouaib Tahtaoui,[‡,▽] Fabrice Guillier,[§,∥] Philippe Klotz,[†,‡] Jean-Luc Galzi,[⊥] Marcel Hibert,[‡] and Brigitte Ilien*[,⊥]

Laboratoire de Pharmacochimie de la Communication Cellulaire, Faculté de Pharmacie, UMR CNRS/ULP 7081, 74 route du Rhin, BP 24, 67401 Illkirch, France, Département Récepteurs et Protéines Membranaires, CNRS UMR 7100, IFR 85, Boulevard Sébastien Brant, BP 10413, 67412 Illkirch, France, and Faust Pharmaceuticals S.A., Bioparc, Boulevard Sébastien Brant, 67400 Illkirch, France

Received May 15, 2005

The efficiency of fluorescence resonance energy transfer (FRET) is dependent upon donor−acceptor proximity and spectral overlap, whether the acceptor partner is fluorescent or not. We report here on the design, synthesis, and characterization of two novel pirenzepine derivatives that were coupled to patent blue VF and pinacyanol dyes. These nonfluorescent compounds, when added to cells stably expressing enhanced green fluorescent protein (EGFP)-fused muscarinic M1 receptors, promote EGFP fluorescence extinction in a time-, concentration-, and atropine-dependent manner. They display nanomolar affinity for the muscarinic receptor, determined using either FRET or classical radioligand binding conditions. We provide evidence that these compounds behave as potent acceptors of energy from excited EGFP with quenching efficiencies comparable to those of analogous fluorescent bodipy or rhodamine red pirenzepine derivatives. The advantages they offer over fluorescent ligands are illustrated and discussed in terms of reliability, sensitivity, and wider applicability of FRET-based receptor binding assays.

Introduction

High-sensitivity methods are increasingly important in biology and medicine and are expected to produce major advances in molecular diagnostics, therapeutics, molecular biology and bioengineering. Fluorescence-based techniques are especially appealing because of the potential sensitivity and specificity that can be achieved (see, for review, refs 1 and 2). Among them, fluorescence resonance energy transfer (FRET), which is intrinsically dependent upon and highly sensitive to proximity changes, represents a powerful monitoring/reporting mechanism for intra- and intermolecular binding events, both in vitro and in vivo.[2−6]

FRET is defined as the nonradiative transfer of the excited-state energy from a donor fluorophore to an acceptor molecule.[7,8] It occurs if the emission spectrum of the donor overlaps the excitation spectrum of the acceptor and FRET efficiency depends on donor−acceptor separation.[7] Thus, any event that brings the two partners closer to (or farther from) each other will lead to a dramatic change in energy transfer and hence fluorescence.

Receptor−ligand interactions, classically studied by separative radioligand binding techniques, are typical bimolecular binding events that can be followed in real time through FRET. Indeed, several G-protein coupled receptors, such as the tachykinin NK2,[9−11] the chemokine CXCR4,[12] and the muscarinic M receptors with their N-termini fused to enhanced green fluorescent protein (EGFP)[13,14] behave as efficient donors for their respective ligands, designed as fluorescent acceptors with appropriate spectral properties. Specific ligand binding is recorded (on living cells and in real time) as a simple variation of EGFP fluorescence emission, giving access (i) to the measurement of kinetic as well as equilibrium parameters of the interaction,[9−14] (ii) to the identification of different interconvertible receptor conformational and functional states,[10,11] and (iii) to the study of allosteric modulators.[14] Finally, miniaturized and automated FRET-based binding assays allow reliable detection of unlabeled competitors under drug screening conditions.[13]

Recently, several publications reported on the use of nonfluorescent acceptors or quenchers such as dabcyl,[15−17] the so-called black hole quenchers BHQ1,[17,18] BHQ2, and QSY-7[17] or QSY-9,[19] nucleotides[17] and especially guanosine,[20,21] or gold nanocrystals.[16,22]

Many of these studies describe molecular beacons (hairpin-shaped oligonucleotides labeled with a fluorophore and a quencher at their extremities) as powerful tools to set up quenching/dequenching hybridization assays.[15,16,18,21] In dual-labeled molecular beacons, the fluorescent reporter and the quencher dye are in such close proximity that they share electrons, transiently forming a nonfluorescent complex that absorbs light energy, which is then dissipated as heat. Thus, very efficient quenching takes place through static quenching,[17,18,22] a mechanism distinct from dynamic Förster resonance energy transfer.[7] Note that static

[†] In fond memory of Dr. Philippe Klotz, our dear friend, colleague, and mentor who died untimely on June 9th, 2005.

* To whom correspondence should be addressed. Mailing address: Département Récepteurs et Protéines Membranaires, CNRS UMR 7100, Ecole Supérieure de Biotechnologie de Strasbourg, Boulevard Sébastien Brant, BP 10413, 67412 Illkirch, France. Tel: 00 33 (0)3 90 24 47 38. Fax: 00 33 (0)3 90 24 48 29. E-mail: ilien@esbs.u-strasbg.fr.

[‡] UMR CNRS/ULP 7081.

[▽] Present adress: Arpida AG, Research & Development of Anti-Infectives, Dammstrasse 36, CH-4142 Muenchenstein, Switzerland.

[§] Faust Pharmaceuticals S.A.

[∥] Present adress: Laboratoires Fournier S.A., 50 rue de Dijon, 21121 Daix, France.

[⊥] CNRS UMR 7100.

10.1021/jm050459+ CCC: $30.25
Published on Web 11/05/2005

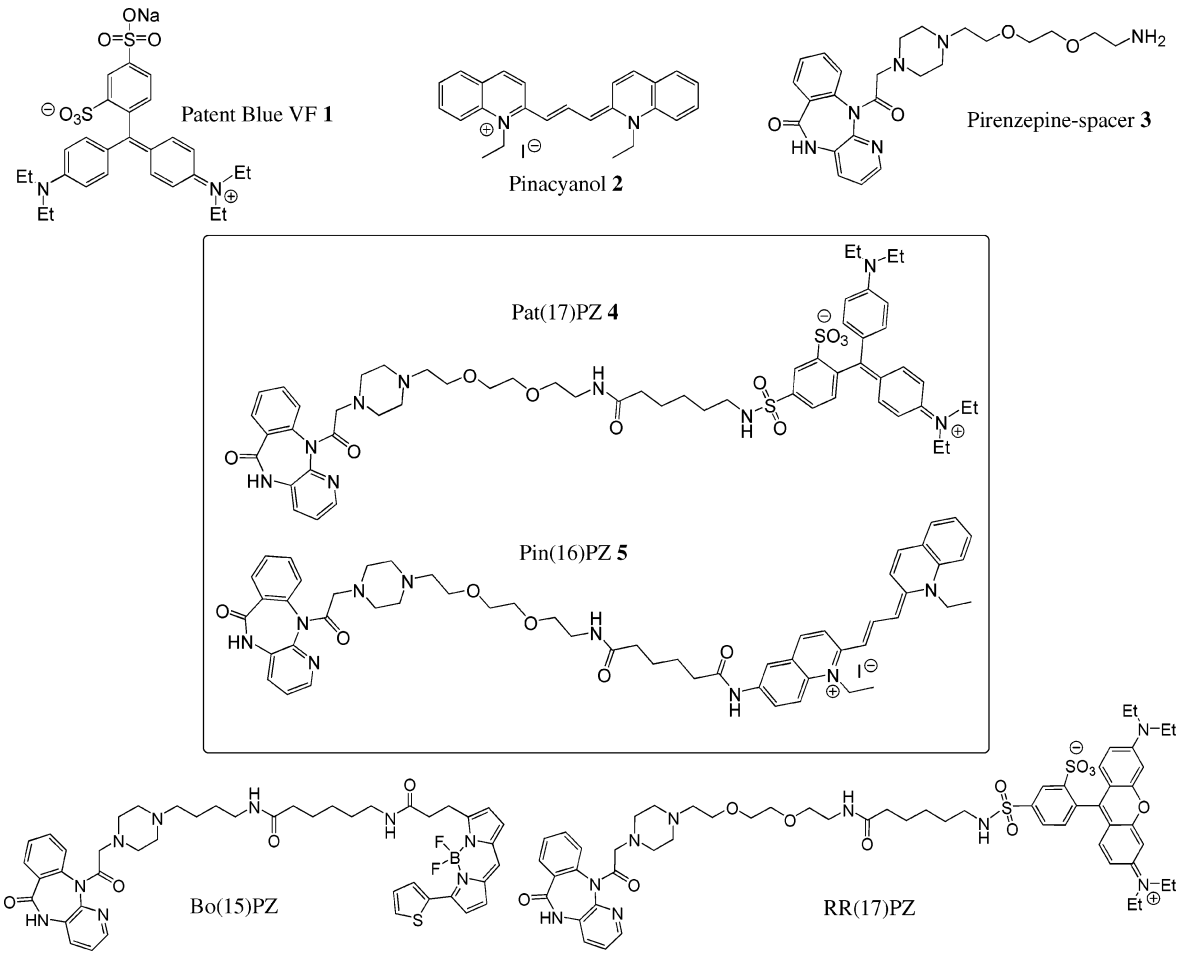

Figure 1. Chemical structures of dyes, dye−pirenzepine derivatives, and fluorescent pirenzepine congeners. Patent blue VF (**1**) and pinacyanol (**2**) are commercially available dyes. The pirenzepine−spacer derivative (**3**)[14] was used for the synthesis of the nonfluorescent pirenzepine derivatives Pat(*17*)PZ, **4**, and Pin(*16*)PZ, **5**. Bo(*15*)PZ and RR(*17*)PZ are, respectively, the bodipy [558/568] and rhodamine red labeled pirenzepine derivatives described in ref 14. For all these pirenzepine derivatives, the value in parentheses specifies the number of atoms (spacer length) separating the chromophore from the pharmacophore, PZ.

quenching efficiency does not depend on spectral overlap between donor fluorescence emission and acceptor absorbance.[17]

Conversely, probe systems that place the two labels at a longer distance (20−100 Å range), that is nevertheless appropriate for FRET require a significant spectral overlap between donor fluorescence emission and quencher absorption for efficient energy transfer to be observed.[17] Available examples for dynamic FRET, quenching include the binding of QSY9-labeled cyclodextrine to fluorescent maltose binding protein (MBP),[19] the use of a series of staggered dual-labeled oligodeoxyribonucleotide hybrids to examine the dependency of quenching efficiency upon donor−quencher separation,[17] the monitoring of retroviral proteases activity using dabcyl-quenched fluorogenic substrates,[23] and the study of hairpin ribozyme kinetics through guanosine-specific quenching of fluorescein-labeled substrates.[20]

The use of nonfluorescent dyes has the particular advantage of eliminating the potential problem of ligand background fluorescence (nonsensitized emission) resulting from direct acceptor excitation. Furthermore, the palette of available quencher molecules offers a great structural diversity,[24] as compared to organic fluorescent probes, allowing the choice of appropriate acceptors over a wide range of maximal absorption wavelengths. From a chemical point of view, quenchers might be also easier to synthesize, using commercially available and often cheaper precursors. Thus, fine structural tuning to get molecules endowed with particular absorption properties prone to quenching optimization should be possible.

Because all of these properties might be beneficial to further improvement of FRET-based receptor binding assays, we decided to examine whether a nonfluorescent ligand could be designed and would behave as an efficient acceptor partner for EGFP, taken as the donor fluorophore. To these ends, we selected the well-established model of muscarinic M1 receptors (EGFP−(Δ17)hM1 chimera) in interaction with the antagonist pirenzepine.[13,14]

Two dyes, patent blue VF (**1**) and pinacyanol (**2**), displaying acceptor-like spectroscopic properties, were coupled to pirenzepine (**3**) to provide Pat(*17*)PZ (**4**) and Pin(*16*)PZ (**5**) probes, respectively (Figure 1). The binding properties of these nonfluorescent derivatives were assessed through FRET and classical [^{3}H]-QNB (Quinuclidinyl Benzilate) competition experiments. Quenching efficiencies were calculated, giving access to the estimation of donor−acceptor separation. Results are discussed in light of those previously obtained, under similar conditions, using fluorescent bodipy (Bo(*15*)PZ) or rhodamine red (RR(*17*)PZ) pirenzepine analogues.[14] Finally, special attention was paid to the critical and

Scheme 1. Synthesis of Functionalized Patent Blue VF, **8**[a]

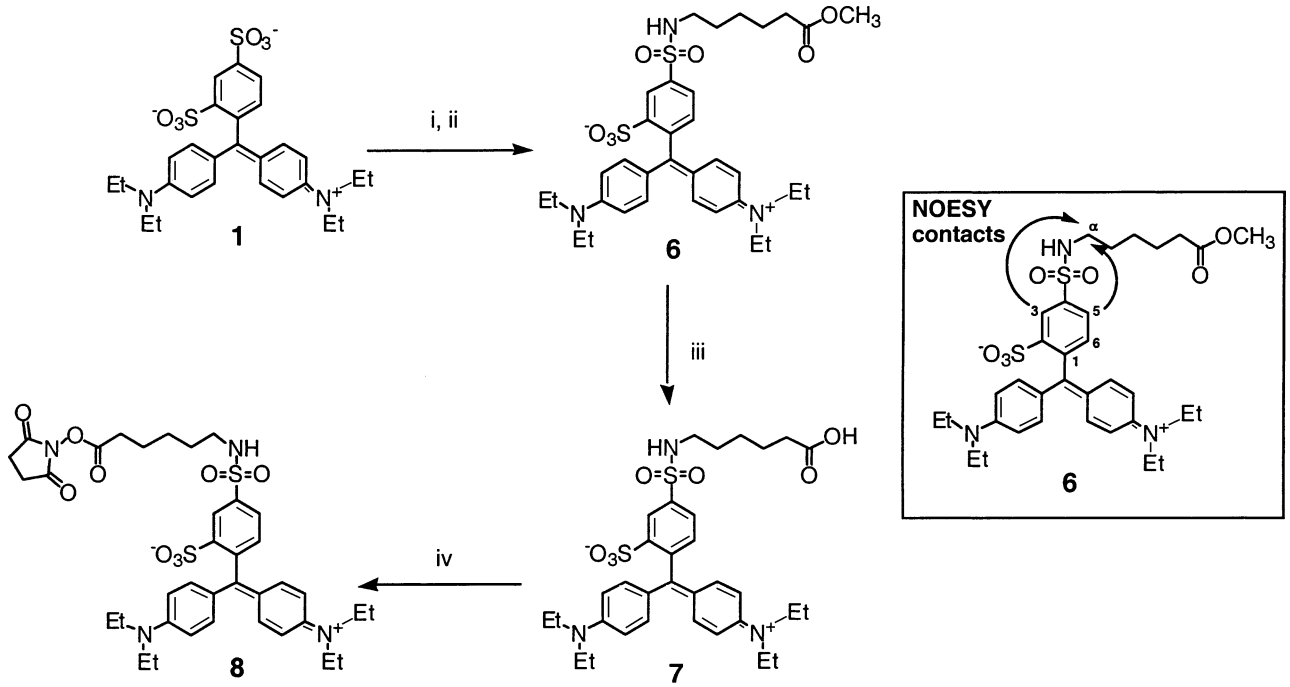

[a] Legend: (i) $POCl_3$, rt, 3 days; (ii) methyl-6-aminohexanoate. HCl, DIEA, DMF, rt, 5 h, 24% (i + ii); (iii) LiOH, dioxane/water (1/1), rt, 1.5 h, 40%; (iv) succinimideOH, DCC, DMF/DME (1/1), 65 °C, 20h, 73%. Inset: 2D-NOESY contacts for compound **6** in a 9:1 $CDCl_3$/CD_3OD mixture.

experimental evaluation of advantages predicted from the use of dye-labeled, instead of fluorescent, derivatives in FRET studies.

Results and Discussion

Two novel donor (EGFP fluorophore)−acceptor (nonfluorescent ligand dye conjugate) pairs have been designed, characterized, and compared for their binding properties and FRET efficiency to EGFP−hM1 muscarinic receptors.

Two dyes, patent blue VF (**1**) and pinacyanol (**2**), were functionalized and coupled to the pirenzepine derivative **3**[14] to give the final nonfluorescent compounds **4** and **5** (Figure 1). The structures of two close fluorescent analogues, the bodipy (Bo(*15*)PZ) and the rhodamine red (RR(*17*)PZ) pirenzepine derivatives,[14] are also presented. For homogeneity purposes, the two pirenzepine conjugates **4** and **5** will be, respectively, referred to as Pat(*17*)PZ and Pin(*16*)PZ, the value in parentheses defining the number of atoms (spacer) separating the pirenzepine pharmacophore from the chromophore molecule.

Synthesis of Nonfluorescent Dye Labeled Pirenzepine Derivatives. Commercially available patent blue VF **1** was first functionalized with methyl-6-aminohexanoate after activation of the *para*-sulfonic acid group with phosphorus oxychloride (Scheme 1), leading to the corresponding methyl ester **6**. This compound was obtained as a single isolated isomer (24% yield). Its 2D-NOESY analysis showed contacts between the α-protons of the methyl-6-aminohexanoate chain and the H3 and H5 protons of the patent blue moiety (Scheme 1 inset). No contacts were found between α-protons and the other protons of the dye moiety, in particular, the H9 and H10 protons. Altogether, these data indicate that the isolated product **6** is the 4-isomer. The ester function of compound **6** was then saponified with LiOH to give the acid **7** in a 40% yield. To prepare the coupling reaction with the pirenzepine derivative **3**, the carboxylic acid function of **7** was then activated as its succinimidyl ester **8** (73% yield).

Because there is no commercially available substituted pinacyanol, we developed a strategy that involves a convergent synthesis through the coupling of the two quinaldinium intermediate molecules **14** and **17** (Scheme 2). The first one (**14**) was obtained in four steps starting from 4-nitroaniline **9** and crotonaldehyde **10**, which were condensed under acidic and biphasic conditions (Doebner−Miller conditions)[25] to give the quinaldine **11**. Reduction of the nitro group afforded the aniline derivative **12**, which was coupled with adipic acid monomethyl ester, activated as its acyl chloride. Quinaldine **13** was thus formed in 87% yield. Pyridine nitrogen was then quaternarized into the first intermediate, quinaldinium ethiodide **14**, using ethyl iodide. Compound **17** was formed in a one-step solvent-free reaction by coupling ethylquinaldinium iodide **15** with *N*,*N*′-diphenylformamidine **16** at 140 °C and was then isolated by recrystallization from ethanol. Finally, condensation of compounds **14** and **17** in acetic anhydride and sodium acetate led to the unsymmetrical pinacyanol **18**. The reaction turned very quickly to dark blue, which is the characteristic color of the cyanine **18**. Final saponification of the ester function provided the corresponding carboxylic pinacyanol acid **19** in 79% yield.

Each of the two functionalized dyes, **8** and **19**, were coupled with the pirenzepine molecule **3** via the amino function of the PEG spacer (Scheme 3). The patent blue VF probe Pat(*17*)PZ (**4**) was formed using classical coupling conditions via succinimidyl ester **8**, diisopropylethylamine, and molecule **3**. For the pinacyanol probe Pin(*16*)PZ (**5**), peptidic coupling conditions through acid

Scheme 2. Synthesis of Functionalized Pinacyanol, **19**[a]

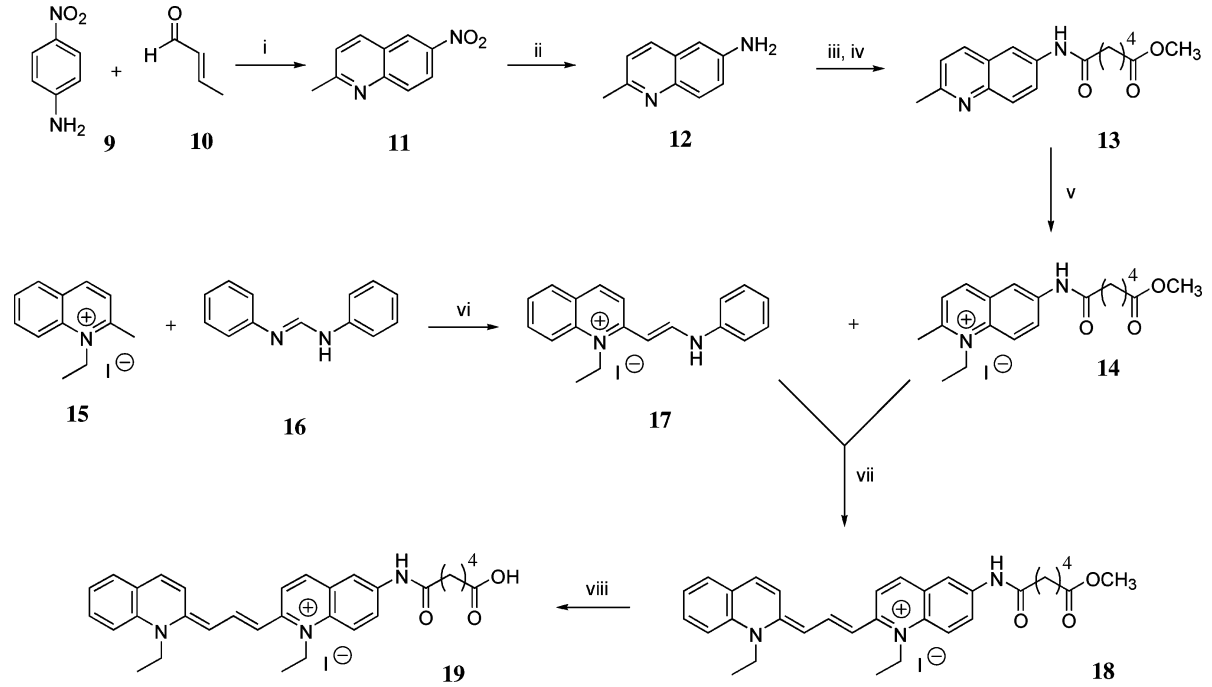

[a] Legend: (i) $PhCH_3$, HCl−6 N, reflux, 2 h, 60%; (ii) $SnCl_2$, HCl, 100 °C, 30 min, 65%; (iii) adipic acid monomethyl ester, $(COCl)_2$, ϵDMF, THF, rt, 1 h; (iv), THF, pyridine, **12**, rt, 2 h, 87% (iii + iv); (v) EtI, $PhCH_3$, sealed tube, 80 °C, 36 h, 46%; (vi) 140 °C, 30 min, 42%; (vii) AcONa, AcOAc, 100 °C, 30 min, then KI, 56%; (viii) K_2CO_3, $MeOH/H_2O/CH_3CN$ (8/1/1), rt, 36 h, 78%.

Scheme 3. Synthesis of the Nonfluorescent Dye Labeled Pirenzepine Derivatives **4** and **5**[a]

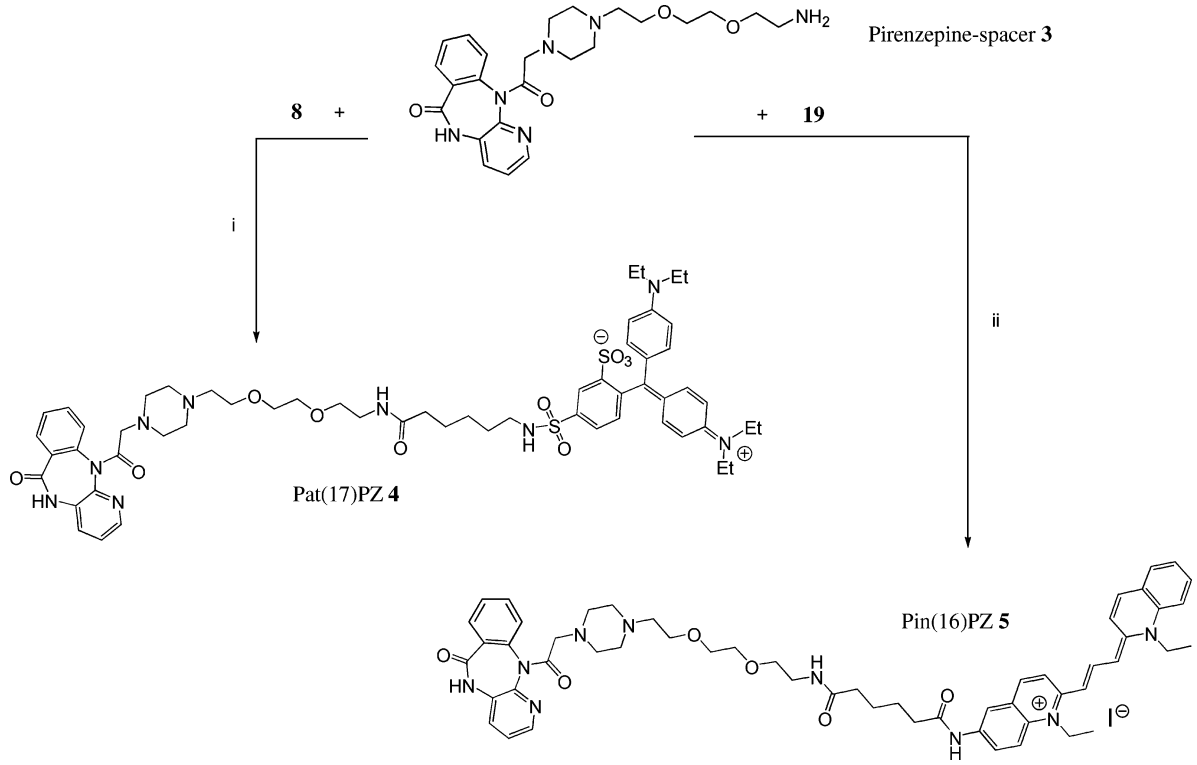

[a] Legend: (i) **8**, DIPEA, CH_3CN/DMF (4/1), 3 h, rt; (ii) **19**, BOP, NMM, DMF, 12 h, rt.

19, BOP reagent, and amine **3** were preferred. Coupling reactions were performed on micromole amounts of the reagents (see Experimental Section) and purification was performed by high-pressure liquid chromatography (HPLC). The expected final products were characterized by mass spectroscopy.

Spectral Properties of Functionalized Dyes and Corresponding Pirenzepine Derivatives. Free patent blue VF (**1**)[26] and pinacyanol (**2**)[27,28] dyes exhibit extremely low quantum yields for fluorescence: 3.7×10^{-4} and 10^{-3}, respectively. Overall spectral properties (maximal absorption wavelength and molecular extinction coefficient) reported for commercial dyes **1** (636 nm; 85 000 $M^{-1}\cdot cm^{-1}$)[24,29] and **2** (604 nm; 175 000 $M^{-1}\cdot cm^{-1}$)[24,28] in MeOH and in water are a priori compatible with those expected for an energy acceptor from excited EGFP.

Since FRET experiments are performed in "physiological" *N*-2-hydroxyethylpiperazine-*N*′-2-ethanesulfonic acid (HEPES) buffer using living cells expressing EGFP-fused muscarinic hM1 receptors, we decided to examine the spectroscopic characteristics of the functionalized dyes alone (**7** and **19**) or coupled to pirenzepine (Pat-(*17*)PZ, **4**, and Pin(*16*)PZ, **5**) both in MeOH and in HEPES/bovine serum albumin (BSA) buffer.

As shown in Figure 2a, the patent blue derivative **7** and its corresponding pirenzepine conjugate **4** (Pat(*17*)-PZ) display identical spectral properties. In HEPES/BSA buffer, as compared to MeOH, a slight 7 nm shift in their maximal absorption wavelength is observed, together with a small decrease in molecular extinction coefficient (Table 1). A similar bathochromic shift (7.5 nm) has been found to occur for the native patent blue VF dye **1** in the presence of RNA aptamers, together with a large increase in fluorescence quantum yield (0.034) most likely due to restricted rotational freedom of the dye within a more viscous environment.[26]

Figure 2b shows that functionalized pinacyanol **19** and Pin(*16*)PZ **5** spectra in MeOH are nearly superimposable. Besides a major peak at 615 nm, they exhibit a band at 570 nm and a small shoulder at 525 nm. Such a broad absorption spectrum, made of three overlapping bands centered at 599−607, 550−570, and 520−525 nm, has also been reported for the native dye **2**, either in MeOH, EtOH, water, or Tris buffer.[24,28,30−32] Interestingly, in HEPES buffer supplemented with BSA (1 mg/mL), the two pinacyanol derivatives display complex blue-shifted absorption spectra with different species in equilibrium (Figure 2b). Indeed, it may be seen in Table 1 that λ_{max} values and associated molecular extinction coefficients for the three main absorbing species that were identified depend on the dilution factor of the stock solutions (0.68 mM in pure DMSO) of pinacyanol **19**, and Pin(*16*)PZ **5**, in the buffer. The reduction in the absorption of the most red-shifted bands, together with the growth of the most energetic band and the overall decrease in absorption intensity of **19** and **5**, is indicative of strong solvatochromic effects (hypsochromy, metachromasia, and hypochromy).[33,34] Such findings are reminiscent of the various and profound rearrangements of pinacyanol spectral properties already described in the literature. Besides its ability to dimerize in solution (ref 31 and references therein), this cationic cyanine dye **2** is known for its high sensitivity to medium polarity and refractive index[28] and for its fluorescence quantum yield that increases up to a value of 0.014 upon binding to dendrimers.[28] It has also proven to be a useful extrinsic probe molecule of aggregation and conformation states of various proteins such as amyloid peptides[31] and ovalbumin.[30] It is noteworthy that spectral changes that are recorded here for pinacyanol derivatives **5** and **19** are very similar to those resulting from the interaction of the native dye **2** with amyloid peptides in a β conformation.[31] One may speculate that the presence of BSA in the buffer that was used here might be involved in the spectral changes that we observed. Indeed, this globular protein has a tendency to aggregate in macromolecular assemblies, which may evolve toward typical β-sheet structures.[35]

Finally, Figure 2c allows us to appreciate the great differences in spectral overlap of absorbance of both

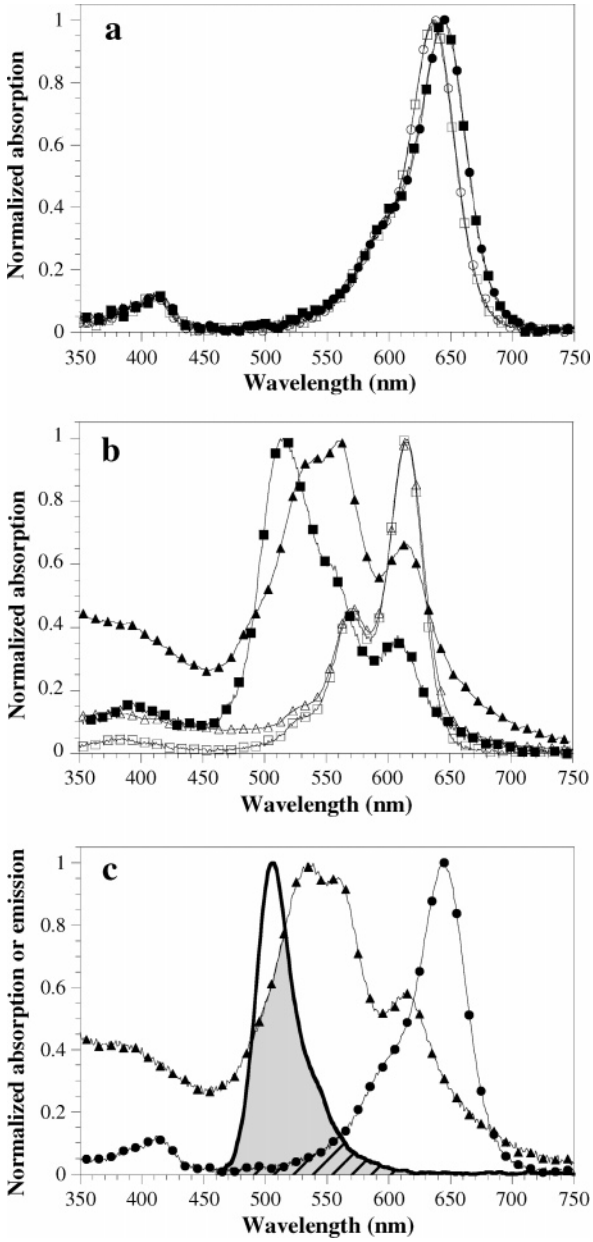

Figure 2. Normalized absorption spectra of dyes and of their pirenzepine derivatives in MeOH and in HEPES/BSA buffer: (a) absorption spectra of the functionalized patent blue VF dye **7** (□,■) and of its pirenzepine derivative Pat(*17*)PZ **4** (○,●) recorded in MeOH (open symbols) and in HEPES/BSA buffer (filled symbols); (b) absorption spectra of functionalized pinacyanol **19** (□,■) and of its pirenzepine conjugate Pin(*16*)PZ **5** (△,▲) recorded in MeOH (open symbols) and in HEPES/BSA buffer (filled symbols; 0.3% final DMSO concentration); (c) superimposition in HEPES/BSA buffer of Pat(*17*)PZ (●) and of Pin(*16*)PZ (▲; 0.5% final DMSO concentration) absorbance with EGFP fluorescence emission (thick line; excitation at 440 nm) with overlaps for normalized spectra shown as hatched or shaded areas, respectively. Maximal absorption wavelengths and corresponding molecular extinction coefficients for Pin-(*16*)PZ were as follows: 534 nm (61 800 $M^{-1}\cdot cm^{-1}$), 559 nm (58 900 $M^{-1}\cdot cm^{-1}$), and 616 nm (36 250 $M^{-1}\cdot cm^{-1}$).

pirenzepine dye derivatives with EGFP fluorescence emission. Spectral overlap integrals (J values) were calculated using absorption spectra obtained with three sets of dilutions of Pat(*17*)PZ and of Pin(*16*)PZ in HEPES/BSA buffer (0.15−0.8% DMSO, v/v). Table 1 indicates that, at least in the probe dilution range that was studied here and corresponds to that used in FRET

Table 1. Spectroscopic Parameters for Dyes and Their Pirenzepine Derivatives

	absorption				donor−acceptor properties	
	MeOH		HEPES/BSA buffer			
compound	λ_{max} (nm)	E ($M^{-1}\cdot cm^{-1}$)	λ_{max} (nm)	E ($M^{-1}\cdot cm^{-1}$)	overlap integral J ($cm^3\cdot M^{-1}$, $\times 10^{-14}$)	Förster radius R_0 (Å)
7	636	85 000	643	78 000	*b*	*b*
Pat(*17*)PZ, **4**	636	85 000	644	78 000	3.5 ± 0.5	38.9 ± 0.8
19 [a]	570	78 700	515 (508)	69 500 (71 400)	*b*	*b*
	615	175 000	557 (558)	41 400 (29 700)		
			608 (607)	26 000 (16 600)		
Pin(*16*)PZ, **5** [a]	571	82 800	541 (531)	61 100 (64 900)	32.9 ± 1.5	56.7 ± 0.4
	615	175 000	562 (556)	64 000 (57 400)		
			617 (611)	43 000 (32 200)		

[a] Absorption parameters in HEPES/BSA buffer were estimated in the presence of an identical 0.3% final DMSO concentration (v/v). Values in parentheses are for a 0.6% (**19**) or a 0.8% (Pin(*16*)PZ) content in DMSO. λ_{max} values and molecular extinction coefficients are reported for all species that were detected. The spectral overlap integral (J), as well as the Förster radius (R_0), was calculated as reported in the Experimental Section. Mean values ± standard deviation are from three independent determinations performed at various dilutions of the dye−pirenzepine derivatives in HEPES/BSA buffer (final DMSO concentrations ranging from 0.15 to 0.8%). [b] Not determined.

Table 2. Binding Properties of Dye Derivatives at EGFP(Δ17)hM1 Receptors[a]

	[^{3}H]-QNB binding	fluorescence resonance energy transfer			
compound	K_i, nM	K_d, nM	amplitude, %	efficiency, E[c]	distance R, Å
pirenzepine[b]	23.5				
7	≫10 000				
19	≫10 000				
Pat(*17*)PZ, **4**	189 ± 40 (n=4)	30.1 ± 4.8 (n=3)	36.9 ± 1.1 (n=4)	0.52 ± 0.02 (n=4)	38.5 ± 0.4 (n=4)
Pin(*16*)PZ, **5**	29.4 ± 9.2 (n=7)	9.1 ± 0.7 (n=6)	35.2 ± 0.7 (n=6)	0.48 ± 0.01 (n=6)	57.4 ± 0.3 (n=6)
Bo(*15*)PZ[b]	69.7	14.2	34.1	0.48	50.3
RR(*17*)PZ[b]	53.5	18.7	48.5	0.68	45.4

[a] Mean values ± standard errors are given for n independent determinations. [b] Values for pirenzepine and for its fluorescent derivatives Bo(*15*)PZ and RR(*17*)PZ are from similarly conducted binding experiments. [14] [c] Efficiency values E were calculated from maximal fluorescence extinction amplitudes (determined at equilibrium with saturating ligand concentrations) and taken to estimate donor−acceptor separation (R values) as reported in the Experimental Section.

experiments, the solvatochromic effects on Pin(*16*)PZ (**5**) absorption properties have little influence on the determination of a mean J parameter with small associated standard deviation. Theoretical donor−acceptor distances (Förster radius; R_0 value) for 50% FRET efficiency were then estimated (Table 1) and pointed to a favorable R_0 value for Pin(*16*)PZ. Moreover, its negligible intrinsic fluorescence properties, added to its broad spectral overlap with donor emission, make probe **5** a good candidate for efficient quenching of EGFP fluorescence. Indeed, such properties are displayed by many efficient dark quenchers,[17−19] but they may also be responsible for inner filter effects.[19] As Pin(*16*)PZ (**5**) significantly absorbs in the maximal EGFP excitation (460 nm) and emission (510 nm) wavelength windows, this possibility has to be considered.

Binding Properties of the Nonfluorescent Ligands at EGFP-Fused M1 Receptors. The interaction of the pirenzepine derivatives with M1 receptors was examined on HEK cells expressing the EGFP(Δ17)hM1 fluorescent chimera.

First, classical radioligand competition experiments were performed with [^{3}H]-QNB to verify the ability of the new compounds to interact with the muscarinic receptor. As reported in Table 2, dye moieties **7** and **19** exhibit very poor binding affinities. In contrast, Pin(*16*)PZ displays a nanomolar K_i-value comparable to that of the antagonist pirenzepine and a 6-fold higher affinity than Pat(*17*)PZ for hM1 receptors. For comparison, Bo(*15*)PZ and RR(*17*)PZ (two closely related fluorescent analogues of the dye derivatives presented here) were found to compete in the 50 nM concentration range with [^{3}H]-QNB for binding to the receptor.[14]

Figure 3 illustrates, through real-time monitoring of EGFP fluorescence emission at 510 nm, several properties of dye **7** and Pat(*17*)PZ binding to EGFP(Δ17)hM1 receptors. When added at an identical 500 nM concentration to the cell suspension (Figure 3a), the derivatized dye **7** leaves the fluorescence signal unchanged, while Pat(*17*)PZ induces a strong and time-dependent fluorescence extinction (up to 38%) reaching equilibrium within 20 min at 21 °C. The small linear drift in basal fluorescence that may be seen with **7** (and also with Pat(*17*)PZ at equilibrium) most probably arises from slow cell settling. Thus, interaction of Pat(*17*)PZ with the EGFP-fused receptor is driven by its pirenzepine moiety, while its patent blue tag does not bind to the receptor per se. The reversible character of Pat(*17*)PZ binding to EGFP−(Δ17)hM1 receptors is illustrated (Figure 3b) by the ability of atropine (at a saturating concentration) to induce a complete recovery in fluorescence emission. Several similar experiments, performed at various Pat(*17*)PZ concentrations, indicated that dissociation followed a monoexponential process with a mean k_{off} value of 0.0008 s^{-1} at 21 °C. Figure 3c visualizes the extent of fluorescence extinction that was achieved at various Pat(*17*)PZ concentrations. As expected, apparent association rates increase with ligand concentration, together with the amplitudes of fluorescence extinction, which, however, stabilize around 35% at 400 nM Pat(*17*)PZ. As an internal control, commercial bodipy [558/568] pirenzepine or Bo(*10*)PZ (one of the most

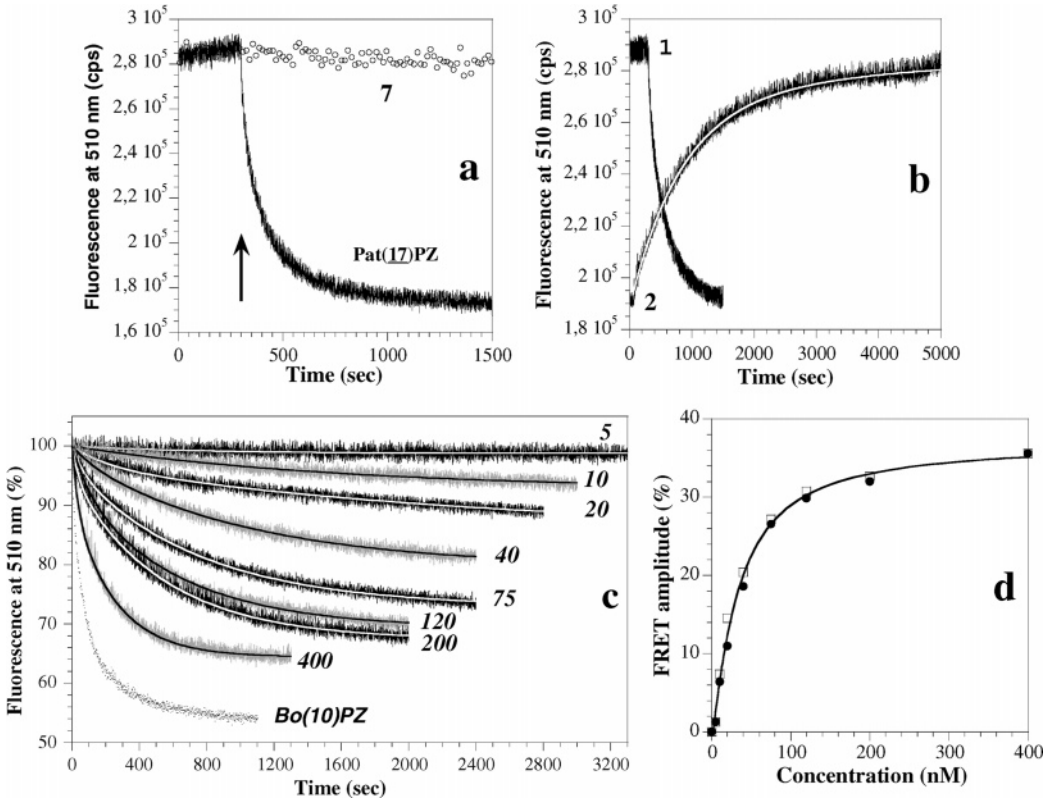

Figure 3. Examination of Pat(*17*)PZ binding properties through real-time monitoring of EGFP emission at 510 nm. In panel a, dye **7** alone (○) or Pat(*17*)PZ (solid line) is added (arrow) at an identical 500 nM concentration to the EGFP(Δ17)hM1 cell suspension. In panel b, Pat(*17*)PZ (150 nM) is added (1) to the cell suspension, and binding is allowed to reach equilibrium. Thereafter, atropine (5 μM) is added to the incubation medium (2) to initiate the dissociation step. Best fit trace (white line) for a monoexponential fluorescence recovery ($k_{off} = 0.001$ s^{-1}) is shown. In panel c, increasing concentrations of Pat(*17*)PZ are added to the EGFP(Δ17)hM1 cell suspension at time 0. Recording durations varied according to equilibrium time. As an internal control, association of the fluorescent pirenzepine derivative Bo(*10*)PZ at 200 nM was also monitored (···). Best fits for an exponential decay of fluorescence are superimposed on each experimental curve. In panel d, amplitudes for maximal fluorescence extinction, either measured at end-point time values of experimental curves shown in Figure 3c (●) or calculated from exponential fitting of the same traces (□), are plotted as a function of Pat(*17*)PZ concentration. Best fit to the empirical Hill equation derived for saturation is drawn. Estimated parameters are maximal FRET amplitude = 37.9% ± 1.8%; $K_d = 33.4 \pm 2.7$ nM; $n_H = 1.20 \pm 0.11$.

potent fluorescent acceptors that we have previously described)[13,14] led at a saturating 200 nM concentration to an expected 46% decrease in fluorescence emission.

Association traces shown in Figure 3c were superimposed with their best exponential fits to derive EGFP fluorescence extinction amplitude values at infinite incubation time. These FRET amplitudes, together with those determined experimentally, were then plotted as a function of Pat(*17*)PZ concentration (Figure 3d). Both determinations were equivalent, indicating that equilibrium was reached at all ligand concentrations. A typical saturation curve was generated, allowing the determination of several parameters such as a maximal FRET amplitude of 37.9% ± 1.8% at saturation, a K_d value of 33.4 ± 2.7 nM and a Hill coefficient of 1.2 ± 0.1.

The second pinacyanol series of ligands was then investigated under similar FRET-based binding conditions. In contrast with the former patent blue VF derivatives, functionalized pinacyanol **19** and Pin(*16*)-PZ both promoted an immediate and concentration-dependent drop in fluorescence upon addition to the cell suspension. This rapid event was followed, exclusively in the presence of Pin(*16*)PZ (as illustrated in Figure 4a, step 1), by a slower time-dependent extinction process that reached equilibrium. Upon addition of 5 μM atropine (step 2), only the slow association component of Pin(*16*)PZ was abolished with a k_{off} of 0.0004 s^{-1} for fluorescence recovery at 21 °C. Accordingly, the sudden decrease of EGFP fluorescence, which was observed using Pin(*16*)PZ (and the inactive derivative **19**, not shown), was not prevented by preincubating the cells with a saturating atropine concentration (step 3) and was thus clearly due to a nonspecific phenomenon. This artifact probably stems from a concentration-dependent inner filter effect of the pinacyanol dyes, which were shown to strongly absorb (Figure 2c) in the excitation/emission wavelength window (460−510 nm) of EGFP.[13] In all subsequent experiments, specific Pin-(*16*)PZ binding was defined as the slow-associating component and more accurately as the amplitude of fluorescence extinction that was sensitive to atropine. Initial fluorescence levels (100%) were thus set, for each probe concentration, as remaining cell fluorescence with fully atropine-occupied receptors (Figure 4a; dashed line). The robustness of this definition is illustrated in Figure 4a both by prevention and dissociation experiments, which indeed led to the determination of an identical FRET amplitude (33.4%) for Pin(*16*)PZ binding at 100 nM. Figure 4b presents the results of six independent saturation experiments and shows that reliable determinations of K_d values (9.1 ± 0.7 nM; $n_H = 1.10 \pm 0.08$) and of maximal FRET amplitudes (35.2% ± 0.7%) for Pin(*16*)PZ binding to hM1 receptors were obtained.

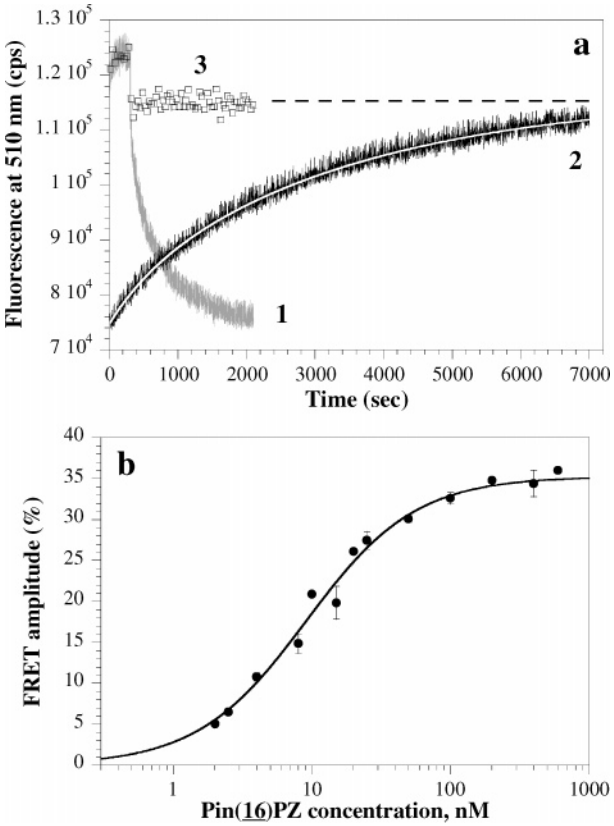

Figure 4. Assessment of receptor specificity for Pin(*16*)PZ-mediated cell fluorescence extinction. In panel a, fluorescence emission (excitation set at 470 nm) of EGFP(Δ17)hM1 cells was monitored in real time following the addition of 100 nM Pin(*16*)PZ (step 1). Subsequent addition of 5 μM atropine (referred to time 0 of dissociation) led to a partial recovery in initial fluorescence with a k_{off} value of 0.004 s^{-1} (step 2). In a separate experiment (□), 100 nM Pin(*16*)PZ was added to cells preincubated with a saturating 5 μM atropine concentration (step 3). Specific FRET amplitude (%) was calculated as the fractional atropine-sensitive extinction of control (dashed line) fluorescence levels. For this typical experiment, a specific FRET amplitude of 33.4% was determined. In panel b, a typical occupancy curve for Pin(*16*)PZ binding to EGFP(Δ17)hM1 receptors was generated by reporting specific FRET amplitudes (mean values with associated standard error bars), which were obtained at various Pin(*16*)PZ concentrations from six independent experiments. Best fit to the empirical Hill equation derived for saturation is drawn (maximal FRET amplitude = 35.2% ± 0.7%; K_d = 9.1 ± 0.7 nM; n_H = 1.10 ± 0.08).

Table 2 summarizes the binding properties of the four nonfluorescent derivatives, together with those of two close fluorescent congeners (Bo(*15*)PZ and RR(*17*)PZ).[14] First, whatever the way used to determine their binding affinity constants, the four pirenzepine derivatives interact with nanomolar affinity with the EGFP(Δ17)-hM1 fluorescent chimera, Pin(*16*)PZ being the most potent among them. As previously discussed, the constant tendency of compounds to exhibit higher affinities when tested by FRET may rely on differences in experimental conditions.[14] Second, it may be observed that maximal FRET amplitudes achieved at saturating concentrations of the two nonfluorescent pirenzepine derivatives and of Bo(*15*)PZ are similar, thereby the corresponding efficiency values *E*. Note, however, that these values did not reach the efficiency afforded with RR(*17*)PZ, the most sensitive fluorescent acceptor that we previously selected.[14]

Estimation of Donor−Acceptor Separation. Because Pat(*17*)PZ (**4**) and Pin(*16*)PZ (**5**) probes display efficiency values for EGFP donor extinction close to 50%, calculation of donor−acceptor separation led to *R* values close to the actual Förster radii (R_0 values) listed in Table 1. Former comparison of a series of bodipy−pirenzepine derivatives, differing by the nature and the length of the spacer introduced between pirenzepine and the fluorophore, led us to propose the existence of a receptor subsite where the bodipy group is locked at a 45−50 Å distance from the EGFP fluorophore.[14]

Here, the distance separating EGFP from receptor-bound pinacyanol in Pin(*16*)PZ is much more difficult to ascertain. Indeed, this dye displays complex spectral properties, which are very sensitive to environmental changes and which probably depend on the free or bound state of the probe.[28,30,31] Such features make the determination of molecular extinction coefficient and R_0 values more uncertain. Because inner filter effects may also interfere with the quantification of a specific EGFP extinction signal, it is clear that the *R* value (57.4 Å) presented here for Pin(*16*)PZ can only be regarded as a rough estimate of the actual donor−acceptor distance.

It remains that all these problems are not encountered with Pat(*17*)PZ. When bound to hM1 receptors, its chromophore is apparently about 7−11 Å closer to EGFP than the bodipy or rhodamine red fluorophores.[14] One may suggest that patent blue VF, due to its overall hydrophilicity, escapes from a putative fluorophore receptor binding pocket and protrudes out of the transmembrane core of the receptor toward the extracellular medium and EGFP.

On the Use of Fluorescent versus Nonfluorescent FRET Acceptors. In the context of FRET-based receptor binding assays, several advantages are expected for quencher-type ligands over fluorescent probes. Of course, this preferentially applies to dye derivatives, such as Pat(*17*)PZ, exhibiting appropriate spectral properties and negligible absorbance at donor excitation wavelength.

A main improvement in the reliability of donor extinction measurements (FRET signal) is expected from the abolition of interfering background acceptor emission, often detectable at micromolar concentrations of fluorescent ligands. This crucial point has been checked (Figure 5) by comparing Bo(*10*)PZ and Pat(*17*)-PZ binding properties at high concentrations. Figure 5a shows that binding of the dye-labeled pirenzepine derivative can be monitored within a concentration range reaching up to 500-fold its K_d value (Figure 3c,d). As expected, association kinetic velocities increase as a function of ligand concentration. Most importantly, amplitudes for EGFP fluorescence extinction at equilibrium are not affected at high dye concentrations (Figure 5a insert) and remain in full agreement with the mean value for maximal FRET amplitude reported for this compound in Table 2. Fluorescence emission spectra recorded on cell suspensions preincubated or not with high Pat(*17*)PZ concentrations indicate too that maximal emission wavelength for EGFP (508 nm) was not shifted upon ligand addition (not shown). Figure 5b depicts a parallel experiment conducted with Bo(*10*)-PZ, which highlights major drawbacks that are associated to the use of a fluorescent probe at high concen-

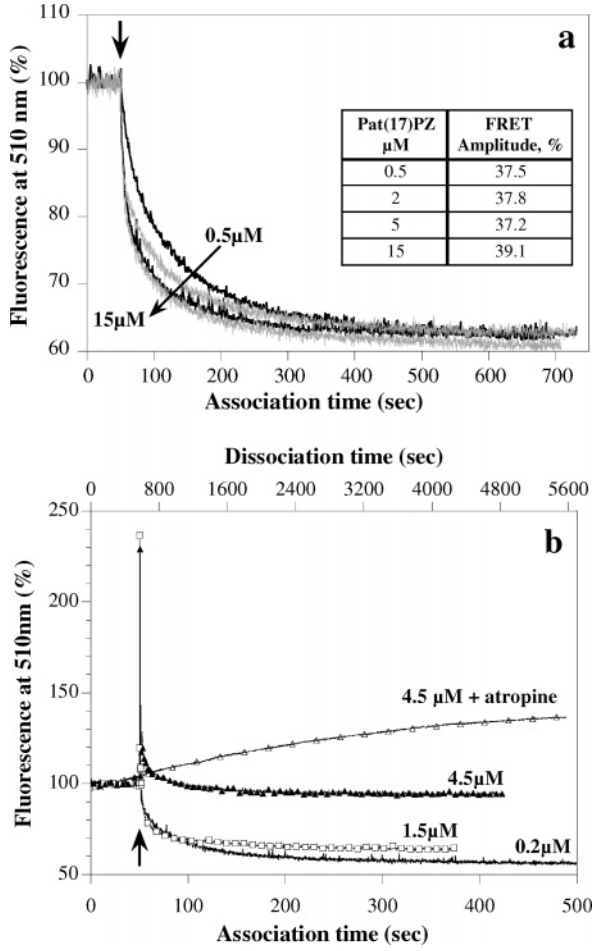

Figure 5. Real-time monitoring of fluorescence emission at 510 nm upon addition of micromolar concentrations of Pat(*17*)PZ and Bo(*10*)PZ to EGFP(Δ17)hM1 expressing cells. Fluorescence at 510 nm (excitation set at 470 nm) was recorded in real time and normalized to 100% for initial cell fluorescence in the absence of ligand. Aliquots of a concentrated stock DMSO solution of Pat(*17*)PZ (a) or of Bo(*10*)PZ (b) were added at 50 s (arrow) to the cell suspension to give the final indicated concentrations. In the inset in panel a, amplitudes for fluorescence extinction at binding equilibrium of Pat(*17*)PZ at various concentrations are given. In panel b, variations in fluorescence emission intensity due to the addition to the cell suspension of Bo(*10*)PZ at 0.2 μM (control), 1.5 μM (□), or 4.5 μM (▲) are shown. Once the fluorescence signal in the presence of 4.5 μM Bo(*10*)PZ was stabilized (around 420 s), atropine (10 μM) was added (time 0; top *x*-axis) to the incubation medium, and fluorescence recovery was recorded with time. The resulting dissociation trace is superimposed with its monoexponential fit (△).

tration. At a 200 nM saturating concentration, Bo(*10*)PZ binding proceeds as expected for a control experiment with a FRET amplitude at equilibrium (44.2%) similar to that obtained in Figure 3c (46%) or previously reported for the same receptor construct (45%).[13,14] In contrast, further increases in the concentration of the fluorescent ligand (up to 45 times the concentration needed to occupy all receptor sites or up to 350-fold its K_d value[13,14]) enable several observations to be made: (i) marked transient injection artifacts due to interfering ligand emission (at 510 nm) at the time of its addition (aliquot of a concentrated stock solution in DMSO) to the cell suspension, (ii) altered kinetics that do not follow mass action and probably result from the superimposition of true ligand binding kinetics to the receptor (EGFP fluorescence extinction) with the time course of the strong Bo(*10*)PZ emission interference, which stabilizes upon ligand homogenization into the incubation medium, and finally (iii) markedly reduced fluorescence extinction amplitudes that represent less than 6% (at 4.5 μM Bo(*10*)PZ) of initial cell fluorescence in the absence of ligand. Thus, at high Bo(*10*)PZ concentrations, direct monitoring of fluorescence emission at 510 nm no longer reflects solely specific ligand binding to EGFP(Δ17)hM1 receptors. Instead, it represents a mixed contribution of both a decrease in EGFP emission (through FRET) and an increase in basal fluorescence levels due to intrinsic ligand emission (with excitation set at 470 nm). This explanation is supported by the findings (Figure 5b) that the addition of atropine (10 μM) to cells equilibrated in the presence of 4.5 μM Bo(*10*)PZ induces a slow recovery in overall fluorescence that reaches a plateau at 145% of initial cell fluorescence at 510 nm. The amplitude (49%) of this monoexponential process is close to that found for EGFP extinction using Bo(*10*)PZ at 200 nM, and its rate constant (0.0003 s^{-1}) is comparable to the off-rate constant (0.0005 s^{-1}) previously defined[14] for Bo(*10*)PZ dissociation from EGFP(Δ17)hM1 receptors.

Altogether, these results highlight the superiority of Pat(*17*)PZ (a derivative that exhibits also negligible absorbance at 470 nm, i.e., the donor excitation wavelength) over Bo(*10*)PZ for performing safe FRET-based binding measurements requiring micromolar concentrations of ligand. As a direct consequence, such nonfluorescent derivatives should help in expanding the number and variety of "FRET-targeted" receptors, including those displaying low-affinity ligand−receptor interactions.

Another strong argument for the use of nonfluorescent versus fluorescent dyes is connected to the environmental dependency of fluorescence quantum yields[8] that may greatly differ for free or specifically or nonspecifically bound probes. Thus, an increase in quantum yield for an acceptor fluorophore could lead to an elevation in its background emission interference. Despite the increase in quantum yield reported for dyes **1** (0.034) and **2** (0.014) when interacting with RNA aptamers[26] and host dendrimers,[28] respectively, such a phenomenon is unlikely to occur with these dyes as their quantum yield values still remain very low.

Though intensity-based FRET detection methods include monitoring the donor intensity, the sensitized acceptor emission, or the ratio between donor and acceptor intensity, it has been found that the fraction of sensitized acceptor emission is hardly detectable in binding assays usually performed at large ligand over receptor molar excess.[9,13] In such a context, dye acceptors may be regarded as equivalent to fluorescent ones because donor emission is the unique parameter that allows reliable and sensitive detection of a FRET process.

Importantly too, nonfluorescent molecules are not subjected to photobleaching, a phenomenon characterized by an irreversible loss of fluorescence properties due to photon-induced chemical damage and covalent modification. Finally and from a more practical point of view, dyes, which are cheaper and probably more stable than fluorophores, may be regarded as interesting tools for high-throughput FRET-based screening methods.

Conclusion

This work demonstrates that ligand−receptor interactions of muscarinic M1 receptors can be monitored and characterized through FRET using a fluorescent donor (EGFP) and a nonfluorescent acceptor. Though a variety of quenchers for various synthetic fluorophores have already been described, [16−18,21] we provide evidence here that dyes, which constitute a wide family of chemicals, may represent appropriate energy acceptors from excited EGFP and possibly also from other GFP variants.

Because donor and acceptor moieties are present on separate molecules, able to form intermolecular receptor−ligand complexes, EGFP extinction most likely relies here on a dynamic Förster mechanism.[8,17,18] This is at variance with most quenchers described in the literature that have been found to act intramolecularly, through a static or contact mode of quenching.[17,18,22]

Pinacyanol and patent blue derivatives of pirenzepine are endowed with high affinity for the muscarinic M1 receptor and quench EGFP fluorescence with efficiencies comparable to those previously reached using fluorescent pirenzepine derivatives.[14] With the example of Pin(*16*)PZ, we show that quenchers that exhibit broad absorption spectra might also lead to undesirable inner filter effects,[19] a problem we circumvented by careful assessment of FRET signal specificity, that is, by monitoring an atropine-sensitive variation in donor emission.

Clearly, Pat(*17*)PZ represents a more suitable compound to get straightforward, reliable, and sensitive measurements of ligand−receptor interactions through FRET. Furthermore the synthesis of other derivatives, displaying greater spectral overlap with donor emission together with minimal absorption at donor excitation wavelength, should help in improving the sensitivity of the method and expanding the panel of "FRET-targeted" receptors. In contrast to binding techniques that make use of a single labeled molecule (either radioactive or fluorescent) and thus require high-affinity ligands, the development of FRET assays using nonfluorescent dye derivatives is expected to lead to broad applications in the receptor field. Indeed, it should give access to the study of low-affinity ligand−receptor interactions (which require micromolar concentrations of probe) while preserving the great receptor specificity of the method arising from donor (EGFP fused to the receptor of interest) extinction measurement. These are very promising conditions that open, for example, the possibility to start the characterization of orphan receptors through the selection of tracer candidates from dye-labeled chemical libraries.

Experimental Section

General Methods. All chemicals were obtained from commercial suppliers and used without further purification.

Patent blue VF [129-17-9] was obtained from ACROS with a 50% dye content. Pyridine was dried over KOH, and DMF was dried on P_2O_5 and distilled from KOH at 70 °C under reduced pressure. Tetrahydrofuran (THF) was distilled from sodium-benzophenone. Acetonitrile (CH_3CN) was distilled from CaH_2. NMR spectra were recorded on a Brucker DPX spectrometer at 200 and 300 MHz (^1H), at 50 and 75 MHz (^{13}C), and at 200 MHz (2D-NOESY). NMR chemical shifts are expressed in ppm relative to internal solvent peaks, and coupling constants (*J*) are measured in hertz. The signals are described as s (singlet), d (doublet), t (triplet), q (quadruplet), m (multiplet), and br s (broad singlet). Electrospray ionization (ESI)-MS were recorded on a Perkin-Elmer Biospec mass spectrometer. MALDI-TOF measurements were carried out on a Brucker BIFLEX spectrometer equipped with the SCOUT high-resolution optics. Silica gel 60 (63−200 μm) from Merck was used for column chromatography. The melting points are measured in open capillary tubes using a Gallekampf apparatus and are uncorrected.

Methyl 6-(4-[(4-Diethylaminophenyl)(4-diethylimino-2,5-cyclohexadien-1-ylidene) methyl]-3-sulfo-1-phenylsulfonamido)hexanoate (6). Phosphorus oxychloride (40 mL) was added to patent blue VF, **1** (50%, 5.66 g, 5.2 mmol), placed in a 100 mL round-bottom flask. The mixture was vigorously stirred at room temperature for 3 days before phosphorus oxychloride was removed under reduced pressure. Toluene was added to the mixture, and $POCl_3$ was removed by azeotropical distillation. The crude oil was then dissolved in DMF (10 mL), and this solution was added dropwise to a solution of methyl-6-aminohexanoate hydrochloride (8.0 g, 44 mmol) and DIPEA (6.45 g, 50 mmol) in DMF (40 mL). The reaction mixture was stirred at room temperature for 5 h, and DMF was evaporated under reduced pressure. The crude resulting product was then taken up in CH_2Cl_2 and washed with water. After separation, the organic layer was concentrated and purified by silica gel column chromatography to give the methyl ester derivative **6** as blue crystals after trituration in Et_2O (0.82 g, 24%). TLC (CH_2Cl_2/MeOH 9/1) R_f 0.6; mp >250 °C; ^1H NMR ($CDCl_3$-10%CD_3OD, 300 MHz) δ 8.55 (d, J = 1.5 Hz, 1H), 7.87 (dd, J_1 = 1.5 Hz, J_2 = 7.5 Hz, 1H), 7.37 (d, J = 9.5 Hz, 4H), 7.11 (d, J = 7.5 Hz, 1H), 6.74 (d, J = 9.5 Hz, 4H), 3.62 (s, 3H), 3.54 (qd, J = 7 Hz, 8H), 2.93 (qd, J = 8 Hz, 2H), 2.28 (t, J = 7.5 Hz, 2H), 1.58−1.52 (m, 4H), 1.34 (m, 2H), 1.26 (t, J = 7 Hz, 12H); ESI-TOF (90 eV) *m/z* calculated 672.28 ($C_{34}H_{46}N_3O_7S_2$), found 672.21 $(M)^+$.

{4-[[4-(5-Carboxy-pentylsulfamoyl)-2-sulfo-phenyl]-(4-diethylamino-phenyl)-methylene]-cyclohexa-2,5-dienylidene}-diethylammonium (7). A solution of lithium hydroxide hydrate (34 mg, 0.81 mmol) in water (10 mL) was added dropwise at room temperature to the methyl ester derivative **6** (170 mg, 0.25 mmol) dissolved in dioxane (10 mL). The reaction was stopped after 1.5 h and before the total conversion of the reaction, because TLC monitoring indicated the formation of a polar side product. The dioxane solvent was removed under reduced pressure, and water (10 mL) was added. The mixture was washed with CH_2Cl_2 (4 times), acidified with a 1 M $KHSO_4$ solution, and extracted with CH_2Cl_2 (5 times) until the aqueous layer became pale red. After concentration of the CH_2Cl_2 layer (without drying over magnesium sulfate), the crude product was purified by silica gel column chromatography to give the carboxylic acid derivative **7** as a blue solid (67 mg, 40%). TLC (CH_2Cl_2/MeOH 9/1), R_f 0.25; mp >250 °C; ^1H NMR (CD_3OD,200 MHz.) δ 8.86 (s, 1H), 8.21 (d, J = 8 Hz, 1H), 7.66 (d, J = 9 Hz; 4H), 7.50 (d, J = 8 Hz, 1H), 7.11 (d, J = 9.4 Hz, 4H), 3.88 (qd, J = 7.2 Hz, 8H), 3.25 (t, J = 6.9 Hz, 2H), 2.53 (t, J = 7.2 Hz, 2H), 1.85−1.76 (m, 4H), 1.65 (m, 2H), 1.58 (t, J = 7.2 Hz, 12H).

[4-((4-Diethylamino-phenyl)-{4-[5-(2,5-dioxo-pyrrolidin-1-yloxycarbonyl)-pentylsulfamoyl]-2-sulfo-phenyl}-methylene)-cyclohexa-2,5-dienylidene]-diethylammonium (8). A mixture of *N*-hydroxysuccinimide (26 mg, 0.226 mmol) and DCC (46 mg, 0.223 mmol) dissolved in DME (5 mL) was added at room temperature onto a solution of the carboxylic acid derivative **7** (65 mg, 0.1 mmol) dissolved in DMF (5 mL). The mixture was stirred at 65 °C for 20 h, and solvents were then removed under reduced pressure. The crude residual product was taken up in CH_2Cl_2 and washed with water. After concentration of the CH_2Cl_2 layer (without drying), the crude product was finally boiled with AcOEt for 5 min and filtered to remove the solubilized DCU. Upon filtration, the succinimidyl ester **8** was recovered as blue crystals, which were washed with hot AcOEt (55 mg, 73%). Mp >250 °C; ^1H NMR ($CDCl_3$ 200 MHz) δ 8.51 (s, 1H), 7.82 (d, J = 7.1 Hz, 1H), 7.31 (d, J =

9.0 Hz, 4H), 7.07 (d, J = 8.1 Hz, 1H), 6.69 (d, J = 8.8 Hz, 4H), 3.47 (qd, J = 6.8 Hz, 8H), 2.89 (t, 2H), 2.75 (s, 4H), 2.52 (t, J = 6.1 Hz, 2H), 1.66 (t, J = 6.1 Hz, 2H), 1.50−1.35 (m, 4H), 1.23 (t, J = 6.6 Hz, 12H).

2-Methyl-6-nitro-quinoline (11). 4-Nitroaniline (616 mg, 4.46 mmol) was dissolved in HCl, 6 N (23 mL), and the mixture was heated at 100 °C. Crotonaldehyde (0.74 mL, 8.92 mmol) in toluene (6 mL) was added dropwise, and the reaction was heated 2 h at 100 °C, then cooled to room temperature and basified with KOH until pH 10−11. The mixture was extracted twice with CH_2Cl_2, and the organic layer was washed with brine and dried over $MgSO_4$. The final quinaldine **11** was obtained after purification by column chromatography on silica gel (503 mg, 60%). TLC (CH_2Cl_2), R_f 0.15; ^{1}H NMR ($CDCl_3$, 200 MHz) δ 8.72 (d, J = 2.7 Hz, 1H), 8.42 (dd, J_1 = 9.3 Hz, J_2 = 2.7 Hz, 1H), 8.20 (d, J = 8.54 Hz, 1H), 8.10 (d, J = 9.3 Hz, 1H), 7.44 (d, J = 8.6 Hz, 1H), 2.79 (s, 3H); ^{13}C NMR ($CDCl_3$, 50 MHz) δ 163.3, 153.6, 150.0, 137.6, 130.4, 125.2, 124.3, 123.9, 122.9, 25.7; ESI-TOF (90 eV) *m/z* calculated 188.06 ($C_{10}H_8N_2O_2$), found 189.05 $(M + H)^+$.

2-Methyl-quinolin-6-ylamine (12). To a solution of compound **11** (500 mg, 2.66 mmol) in HCl, 1 N (20 mL), a solution of $SnCl_2$ (2.52 g, 13.3 mmol) in HCl, 1 N (10 mL), was added. The mixture was heated at 100 °C during 15 min and then cooled to room temperature. The precipitate was filtered, washed with a solution of KOH (1 N) until pH 11−12, and extracted with AcOEt. After removal of the solvent under reduced pressure, the expected compound was purified by silica gel column chromatography to afford **12** as a white solid (274 mg, 65%). TLC (AcOEt), R_f 0.28; ^{1}H NMR ($CDCl_3$, 200 MHz) δ 7.81 (d, J = 8.8 Hz, 1H), 7.77 (d, J = 7.6 Hz, 1H), 7.12 (t, J = 6.6 Hz, 2H), 6.84 (d, J = 1.7 Hz, 1H), 3.88 (br s, 2H), 2.65 (s, 3H); ^{13}C NMR ($CDCl_3$, 50 MHz) δ 155.1, 143.9, 142.9, 134.1, 129.7, 127.8, 122.2, 121.3, 107.7, 24.9.

Methyl 6-[(2-Methylquinolin-6-yl) amino]-6-oxohexanoate (13). To a solution of the adipic acid monomethyl ester (324 mg, 2.02 mmol) in THF (10 mL), oxalyl chloride (0.175 mL, 2.02 mmol) was added dropwise. A few drops of DMF (0.1 mL) was added to the mixture. Stirring was continued 1 h at room temperature; then the reaction mixture was evaporated to dryness. The crude product was dissolved in THF (10 mL); then pyridine was added (0.615 mL, 7.6 mmol), followed by the compound **12** (200 mg, 1.26 mmol). The reaction mixture was stirred 2 h at room temperature, then washed with HCl, 0.5 N, and extracted with AcOEt. The organic layers were washed with brine, dried over $MgSO_4$, filtered, and evaporated. The final product was obtained after purification by column chromatography on silica gel (331 mg, 87%). TLC (CH_2Cl_2/AcOEt 5/5). R_f 0.30; ^{1}H NMR ($CDCl_3$, 200 MHz) δ 8.35 (d, J = 1.96 Hz, 1H), 7.99 (t, J = 8.55 Hz, 2H), 7.76 (br s, 1H), 7.54 (dd, J_1 = 9.04 Hz, J_2 = 2.44 Hz, 1H), 7.27 (d, J = 8.54 Hz, 1H), 3.70 (s, 3H), 2.73 (s, 3H), 2.37−2.49 (m, 4H), 1.74−1.82 (m, 4H); ^{13}C NMR ($CDCl_3$, 50 MHz) δ 174.1, 171.3, 157.8, 144.6, 136.3, 135.4, 128.7, 127.0, 125.9, 123.2, 122.6, 116.1, 51.6, 37.1, 33.6, 24.8, 24.2; ESI-TOF (90 eV) *m/z* calculated 300.14 ($C_{17}H_{20}N_2O_3$), found $(M + H)^+$ 301.13.

1-Ethyl-6-[(6-methoxy-6-oxohexanoyl) amino]-2-methylquinolinium Iodide (14). Compound **13** (100 mg, 0.33 mmol) dissolved in anhydrous toluene (3 mL) with ethyl iodide (54 μL, 0.66 mmol) was heated in a sealed tube at 80 °C during 36 h. The reaction mixture was evaporated to dryness under reduced pressure, and the crude product was triturated in AcOEt. The precipitate was filtered off, washed several times with AcOEt, and dried under high vacuum to give compound **14** as a pinkish solid (70 mg, 46%). ^{1}H NMR (DMSO, 200 MHz) δ 10.82 (br s, 1H), 9.03 (d, J = 8.3 Hz, 1H), 8.77 (s, 1H), 8.62 (d, J = 9.52 Hz, 1H), 8.25 (d, J = 9.04 Hz, 1H), 8.07 (d, J = 8.8 Hz, 1H), 4.96 (q, J = 7.08 Hz, 2H), 3.61 (s, 3H), 3.11 (s, 3H), 2.38−2.47 (m, 4H), 1.52−1.65 (m, 7H); ^{13}C NMR (DMSO, 50 MHz) δ 173.2, 172.1, 157.9, 144.8, 139.1, 134.3, 129.2, 127.7, 125.7, 119.8, 116.0, 51.2, 47.2, 36.0, 24.1, 24.0, 22.0, 13.5.

2-[(*E*)-2-Anilinovinyl]-1-ethylquinolinium Iodide (17). Quinaldine ethiodide **15** (500 mg, 1.67 mmol) and *N*,*N*′-diphenylformamidine **16** (328 mg, 1.67 mmol) were vigorously stirred under argon at 140 °C during 30 min. The obtained brownish solid was then recrystallized from HCl, 2 N. The yellow solid **17** was then filtered off and dried under vacuum (280 mg, 42%). ^{1}H NMR (DMSO, 200 MHz) δ 11.62 (br s, 1H), 8.97 (d, J = 11.7 Hz, 1H), 8.38 (q, J = 8.5 Hz, 2H), 8.12 (d, J = 9.1 Hz, 1H), 8.02 (d, J = 8.1 Hz, 1H), 7.89 (t, J = 7.8 Hz, 1H), 7.62 (t, J = 7.34 Hz, 1H), 7.38−7.52 (m, 4H), 7.15 (t, J = 7.1 Hz, 1H), 6.45 (d, J = 11.7 Hz, 1H), 4.57 (q, J = 6.8 Hz, 2H), 1.48 (t, J = 7.1 Hz, 3H); ^{13}C NMR (DMSO, 50 MHz) δ 155.3, 149.4, 139.5, 138.4, 137.9, 133.1, 129.7, 129.6, 125.1, 124.4, 119.0, 117.1, 116.9, 94.2, 44.3, 12.4; ESI-TOF (90 eV) *m/z* calculated 402.06 ($C_{19}H_{19}IN_2$), found 275.15 $(M - I)^+$.

1-Ethyl-2-[(1*E*,3*E*)-3-(1-ethylquinolin-2(1*H*)-ylidene) Prop-1-enyl-6-[(6-methoxy-6-oxo-hexanoyl) amino] Quinolinium Iodide (18). A mixture of compound **14** (70 mg, 0.15 mmol), compound **17** (68 mg, 0.17 mmol), and anhydrous sodium acetate (25 mg, 0.31 mmol) in acetic anhydride (5 mL) was heated at 100 °C during 30 min. The mixture changes color rapidly to dark blue, which is the characteristic color of the cyanine dye. The final compound **18** was then precipitated by addition of a saturated aqueous solution of KI. The solid was filtered off, washed with water, and dried under reduced pressure (55 mg, 56%). ^{1}H NMR (DMSO, 300 MHz) δ 9.80 (br s, 1H), 8.56 (t, J = 11.3 Hz, 1H), 7.40−8.15 (m, 11H), 6.46−6.59 (m, 2H), 4.50 (q, J = 9 Hz, 4H), 3.63 (s, 3H), 2.38 (m, 4H), 0.88−1.70 (m, 10H); ^{13}C NMR (DMSO, 75 MHz) δ 172.4, 170.8, 150.9, 146.2, 138.3, 135.9, 135.3, 134.3, 131.6, 128.4, 124.2, 124.0, 123.8, 119.8, 119.6, 117.0, 116,2, 115.1, 105.1, 104.0, 50.4, 42.5, 42.0, 35.5, 32.6, 23.9, 23.5, 12.0, 11.7; ESI-TOF (90 eV) *m/z* calculated 637.18 ($C_{32}H_{36}IN_3O_3$), found 510.25 $(M - I)^+$.

6-[(5-Carboxypentanoyl) amino]-1-ethyl-2-[(1*E*,3*E*)-3-(1-ethylquinolin-2 (1*H*)-ylidene) prop-1-enyl] Quinolinium Iodide (19). Compound **18** (50 mg, 0.0785 mmol) was dissolved in a mixture of MeOH/H_2O/CH_3CN (8/1/1, 10 mL), and K_2CO_3 (22 mg, 0.157 mmol) was added. The reaction was stirred during 36 h at room temperature. The reaction mixture was then evaporated to dryness under reduced pressure, and water was added (10 mL). The pH of the obtained solution was then rectified to 4−5 by addition of HCl, 1 N. The obtained precipitate was filtered off and dried under high vacuum to give compound **19** as a blue solid (38 mg, 78%). ^{1}H NMR (DMSO, 200 MHz) δ 12.03 (br s, 1H), 10.23 (br s, 1H), 8.58 (t, J = 11.9 Hz, 1H), 8.22 (t, J = 11.7 Hz, 2H), 7.67−8.00 (m, 7H), 7.36 (t, J = 7.2 Hz, 1H), 6.56 (d, J = 12 Hz, 1H), 6.45 (d, J = 11.5 Hz, 1H), 4.40 (q, J = 7.3 Hz, 4H), 2.25−2.35 (m, 4H), 1.01−1.60 (m, 10H); ^{13}C NMR (DMSO, 75 MHz) δ 174.3, 171.4, 151.2, 151.1, 146.7, 138.6, 136.3, 135.8, 134.8, 134.3, 131.1, 128.9, 125.2, 124.4, 124.2, 120.3, 120.0, 126.9, 125.7, 105.6, 104.5, 43.0, 42.6, 36.1, 33.4, 24.6, 24.1, 12.7, 12.4.

Preparation of the Nonfluorescent Dye Labeled Pirenzepine Derivatives 4 and 5. The dye-labeled derivatives were obtained by coupling the spacer-linked pirenzepine **3** dissolved in dry DMF with the corresponding dye at room temperature (Scheme 3). The reaction was monitored by HPLC and stopped upon complete disappearance of the dye reagent (after 3 h for compound **8** (probe **4**) and 12 h for compound **19** (probe **5**)). The products were purified under reversed-phase HPLC conditions (as detailed below) and eluted at retention time t_r. The fractions of interest were pooled, concentrated in a Speed Vac concentrator (ISS 100 Savant), and further checked for purity by analytical HPLC (using different elution conditions as reported below). They were all found to elute as single symmetrical peaks at retention time t_r. The identities of the compounds were analyzed by MALDI-TOF or ESI-TOF.

2{[4-(Diethylamino)phenyl][4-(diethyliminio)cyclohexa-2,5-dien-1-ylidene]methyl}-5-({[6-oxo-6-({2-[2-(2-{4-[2-oxo-2-(6-oxo-5,6-dihydro-11*H*-pyrido[2,3-*b*]1,4benzodiazepin-11-yl) ethylpiperazin-1-yl}ethoxy)ethoxy]ethyl}amino)-hexyl]amino}sulfonyl)]-benzenesulfonate (4). A solution of DIPEA (0.5 mL of 14.5 mM, 7.2 μmol) was added to a suspension of the pirenzepine derivative **3** (2.2 mg, 2.67 μmol) in CH_3CN (1 mL). Solubilization was achieved with DMF (0.5 mL). A solution of succinimidyl ester **8** (2 mg, 2.65 μmol) in

CH_3CN (1 mL) was added upon stirring at room temperature, and the reaction was monitored by TLC for the appearance of a polar product ($MeOH/CH_2Cl_2$ 2/8, R_f 0.15). After 3 h at room temperature, the reaction was stopped, and the solvents were removed under reduced pressure. Semipreparative HPLC was performed using a C_{18} Dionex Vydac column (22 mm × 250 mm; 300 Å; 15 μm) equilibrated in solvent A (H_2O 70%/MeOH 30%/TFA 0.05%; v/v) and eluted with a linear gradient from 0 to 100% of solvent B (MeOH 100%/TFA 0.05%; v/v) in 38 min at a flow rate of 10 mL/min. This allowed the determination of a t_r of 25.8 min for **4** and its isolation as a blue product (1.0 mg, 34% yield). Its purity (around 93%) was then confirmed by two different analytical HPLC runs with absorbance monitored at 220 and 600 nm. First, using a Zorbax Eclipse C_{18} column (150 mm × 4.6 mm) equilibrated in solvent A (MeOH 30%/H_2O 70%/AcOH 0.5%; v/v), elution proceeded with a linear gradient from 0 to 100% of solvent B (MeOH) in 40 min at a flow rate of 0.5 mL/min (t_r = 23.6 min). The second system involved a Waters Nova-Pack C_{18} column (150 mm × 3.9 mm; 60 Å; 4 μm) equilibrated in solvent A (H_2O 90%/CH_3CN 10%/TFA 0.05%; v/v) and eluted with a linear gradient from 0 to 100% solvent B (H_2O 10%/CH_3CN 90%/TFA 0.05%; v/v) in 60 min at a flow rate of 1 mL/min. A t_r of 30.0 min was found for **4**. ESI-TOF *m/z* calculated 1108.50 ($C_{57}H_{74}N_9O_{10}S_2$), found 1108.44 $(M + H)^+$, 554.70 $[(M + 2H)^+]/2$.

1-Ethyl-2-[(1*E*,3*E*)-3-(1-ethylquinolin-2 (1*H*)-ylidene) prop-1-enyl]-6{[6-oxo-6-({2-[2-(2-{4-[2-oxo-2-(6-oxo-5,6-dihydro-11*H*-pyrido [2,3-*b*][1,4]benzodiazepin-11-yl)ethyl]-piperazin-1-yl}ethoxy)ethoxy]ethyl}amino)hexanoyl]-amino}] Quinolinium Iodide (5). To a solution of compound **19** (5 mg, 8.02 μmol) in anhydrous DMF (3 mL), BOP (4.61 mg, 10.4 μmol) and NMM (1.14 μL, 10.4 μmol) were added. The mixture was stirred for 30 min at room temperature before the addition of the derivative **3** (4.45 mg, 8.82 μmol). Stirring was pursued for 12 h at room temperature. After AcOEt addition, the precipitate was filtered off and washed with AcOEt. HPLC purification of the colored probe **5** was performed on a Zorbax reversed-phase C_{18} column (250 mm × 4.6 mm) using an isocratic elution mode (CH_3CN 35%, H_2O 65%, TFA 0.1%; v/v) for 30 min at a flow rate of 1 mL/min (t_r = 22.0 min). The second system involved a Waters Nova-Pack C_{18} column (150 mm × 3.9 mm; 60 Å; 4 μm) and elution conditions identical to those previously detailed for **4** and led here to the determination of a t_r of 38.3 min for compound **5**. MALDI-TOF *m/z* calculated 1073.40 ($C_{55}H_{64}IN_9O_6$), found 946.50 $(M - I^-)^+$.

Expression of EGFP(Δ17)hM1 Receptors. HEK 293 cells with stable expression of the EGFP(Δ17)hM1 construct (600 fmol of sites per 10^6cells) were obtained as described.[13]

[^{3}H]-QNB binding assays. Competition experiments were performed using intact EGFP(Δ17)hM1 expressing cells suspended in HEPES/BSA buffer (10 mM HEPES, 137.5 mM NaCl, 1.25 mM $MgCl_2$, 1.25 mM $CaCl_2$, 6 mM KCl, and 10 mM glucose, pH 7.4; supplemented with 1 mg/mL bovine serum albumin). Incubation proceeded at 37 °C for 1 h in the presence of [^{3}H]-QNB (250 pM), of various concentrations of compounds to be tested, or of 4 μM atropine for nonspecific binding measurement. K_i values of competitors were calculated from IC_{50} values as reported.[13]

Spectroscopy. UV−visible absorbance spectroscopy was done with a Cary 1E (Varian) spectrophotometer.

Absorption spectra for compounds, diluted either in MeOH or in HEPES/BSA buffer (pH 7.4), were recorded in the 350−750 nm wavelength range. Fluorescence measurements were made using a SPEX Fluorolog 2 (Jobin Yvon Horiba) spectrofluorimeter equipped with a 450W Xe lamp. Data were stored using the DM3000 software provided with the spectrofluorimeter.

Real-time fluorescence measurements. Experiments were conducted at 21 °C as previously detailed.[13,14] Briefly, EGFP(Δ17)hM1 cells were suspended in HEPES/BSA buffer (typically at 2 10^6 cells/mL), placed in a 1-mL thermostated (21 °C) quartz cuvette with magnetic stirring and recorded for fluorescence emission at 510 nm (excitation set at 470 nm). Variations of this signal upon dye-labeled ligand addition (usually 4 μL of a 250-fold concentrated DMSO stock) were followed in real time. Occupancy curves were generated by plotting amplitudes for fluorescence extinction (in percent) at equilibrium as a function of ligand concentration. K_d values and maximal FRET amplitudes were from data fitting to the empirical Hill equation derived for saturation. Dissociation traces were fit according to a monoexponential decay of fluorescence to derive off-rate constants. Mathematical analyses were done using Kaleidagraph 3.08 (Synergy Software).

Estimation for Donor−Acceptor Distances. The distance R_0 (Förster radius) for 50% energy transfer efficiency E, the spectral overlap integral J for the combined emission of EGFP and dye absorbance, and the donor−acceptor separation R were calculated as previously described.[9,13−14] Briefly, R_0 (Å) was calculated from the equation[8] $R_0 = 9790(\kappa^2 N^{-4} \Phi_D J)^{1/6}$ with κ^2, N and Φ_D parameters taken to be, respectively, $^2/_3$, 1.4, and 0.66.

The distance R (Å) between EGFP and the dye moiety of bound ligands was estimated using Förster's equation:[7] $R = R_0(1/E - 1)^{1/6}$. The efficiency of fluorescence energy transfer (E) was defined as the fractional decrease in specific EGFP fluorescence due to ligand binding, that is, maximal FRET amplitude (%) achieved at a saturating ligand concentration corrected for nontransfected cell autofluorescence.

Acknowledgment. This work was supported by the Centre National de la Recherche Scientifique, the Institut National de la Santé et de la Recherche Médicale, the Université Louis Pasteur, the Ministère de la Recherche (ACI 2002), IFR 85, and Hoechst-Marion-Roussel (fellowship to C.T.). We are grateful to Dr. J. Garwood for critical reading of the manuscript and to Dr. D. Bonnet and C. Antheaume for their valuable contribution to NMR studies.

Supporting Information Available: A table listing the formulas, molecular and isotopic weights, MALDI-TOF analyses, and HPLC elution times for compounds **4**, **5**, **7**, and **19** and ^{1}H NMR and 2D-NOESY NMR spectra and analyses for compound **6**. This material is available free of charge via the Internet at http://pubs.acs.org.

References

(1) Hovius, R.; Vallotton, P.; Wohland, T.; Vogel, H. Fluorescence techniques: shedding light on ligand−receptor interactions. *Trends Pharmacol. Sci.* **2000**, *21*, 266−273.
(2) Zhang, J.; Campbell, R. E.; Ting, A. Y.; Tsien, R. Y. Creating new fluorescent probes for cell biology. *Nat. Rev. Mol. Cell. Biol.* **2002**, *3*, 906−918.
(3) Szöllosi, J.; Damjanovich, S.; Matyus, L. Application of fluorescence resonance energy transfer in the clinical laboratory: routine and research. *Cytometry* **1998**, *34*, 159−179.
(4) Selvin, P. R. The renaissance of fluorescence resonance energy transfer. *Nat. Struct. Biol.* **2000**, *7*, 730−734.
(5) Lilley, D. M. J.; Wilson, T. J. Fluorescence resonance energy transfer as a structural tool for nucleic acids. *Curr. Opin. Chem. Biol.* **2000**, *4*, 507−517.
(6) Miyawaki, A. Visualization of the spatial and temporal dynamics of intracellular signaling. *Dev. Cell* **2003**, *4*, 295−305.
(7) Förster, T. Zwischenmolekulare Energiewanderung und Fluoreszenz. *Ann. Phys. (Leipzig)* **1948**, *2*, 55−75.
(8) Lakowicz, J. R. *Principles of fluorescence spectroscopy*; Kluwer Academic/Plenum Press: New York, 1999.
(9) Vollmer, J. Y.; Alix, P.; Chollet, A.; Takeda, K.; Galzi J.-L. Subcellular compartmentalization of activation and desensitization of responses mediated by NK2 neurokinin receptors. *J. Biol. Chem.* **1999**, *274*, 37915−37922.
(10) Palanché, T.; Ilien, B.; Zoffmann, S.; Reck, M.-P.; Bucher, B.; Edelstein, S. J.; Galzi, J.-L. The neurokinin A receptor activates calcium and cAMP responses through distinct conformational states. *J. Biol. Chem.* **2001**, *276*, 34853−34861.
(11) Lecat, S.; Bucher, B.; Mely, Y.; Galzi, J.-L. Mutations in the extracellular amino-terminal domain of the NK2 neurokinin receptor abolish cAMP signaling but preserve intracellular calcium responses. *J. Biol. Chem.* **2002**, *277*, 42034−42048.

(12) Valenzuela-Fernandez, A.; Palanché, T.; Amara, A.; Magerus, A.; Altmeyer, R.; Delaunay, T.; Virelizier, J.-L.; Baleux, F.; Galzi, J.-L.; Arenzana-Seisdedos, F. Optimal inhibition of X4 HIV isolates by the CXC chemokine stromal cell-derived factor 1α requires interaction with cell surface heparan sulfate proteoglycans. *J. Biol. Chem.* **2001**, *276*, 26550−26558.
(13) Ilien, B.; Franchet, C.; Bernard, P.; Morisset, S.; Weill, C. O.; Bourguignon, J.-J.; Hibert, M.; Galzi, J.-L. Fluorescence resonance energy transfer to probe human M1 muscarinic receptor structure and drug binding properties. *J. Neurochem*. **2003**, *85*, 768−778.
(14) Tahtaoui, C.; Parrot, I.; Klotz, P.; Guillier, F.; Galzi, J.-L.; Hibert, M.; Ilien, B. Fluorescent pirenzepine derivatives as potential bitopic ligands of the human M1 muscarinic receptor. *J. Med. Chem*. **2004**, *47*, 4300−4315.
(15) Tyagi, S.; Marras, S. A. E.; Kramer, F. R. Wavelength-shifting molecular beacons. *Nat. Biotechnol.* **2000**, *18*, 1191−1196.
(16) Dubertret, B.; Calame, M.; Libchaber, A. J. Single-mismatch detection using gold-quenched fluorescent oligonucleotides. *Nat. Biotechnol*. **2001**, *19*, 365−370.
(17) Marras, S. A. E.; Kramer, F. R.; Tyagi, S. Efficiencies of fluorescence resonance energy transfer and contact-mediated quenching in oligonucleotide probes. *Nucleic Acids Res.* **2002**, *30*, e122.
(18) Johansson, M. K.; Fidder, H.; Dick, D.; Cook, R. M. Intramolecular dimers: A new strategy to fluorescence quenching in dual-labeled oligonucleotide probes. *J. Am. Chem. Soc.* **2002**, *124*, 6950−6956.
(19) Medintz, I. L.; Goldman, E. R.; Lassman, M. E.; Mauro, J. M. A fluorescence resonance energy transfer sensor based on maltose binding protein. *Bioconjugate Chem.* **2003**, *14*, 909−918.
(20) Walter, N. G.; Burke, J. M. Real-time monitoring of hairpin ribozyme kinetics through base-specific quenching of fluorescein-labeled substrates. *RNA* **1997**, *3*, 392−404.
(21) Knemeyer, J.-P.; Marmé, N.; Sauer, M. Probes for detection of specific DNA sequences at the single-molecule level. *Anal. Chem*. **2000**, *72*, 2717−3724.
(22) Maxwell, D. J.; Taylor, J. R., Nie, S. Self-assembled nanoparticle probes for recognition and detection of biomolecules. *J. Am. Chem. Soc.* **2002**, *124*, 9606−9612.
(23) Matayoshi, E. D.; Wang, G. T.; Kraft, G. A.; Erickson, J. Novel fluorogenic substrates for assaying retroviral proteases by resonance energy transfer. *Science* **1990**, *247*, 954−958.
(24) Green, F. J. *Sigma-Aldrich Handbook of Stains, Dyes and Indicators*; Aldrich Chemical Co., Inc.: Milwaukee, WI, 1990.
(25) Matsugi M.; Tabusa F.; Minamikawa J.-I. Doebner-Miller synthesis in a two phase system: practical preparation of quinolines. *Tetrahedron Lett.* **2000**, *41*, 8523−8525.
(26) Babendure, J. R.; Adams, S. R.; Tsien, R. Y. Aptamers switch on fluorescence of triphenylmethane dyes. *J. Am. Chem. Soc.* **2003**, *125*, 14716−14717.
(27) Rentsch, S.; Danielius, R.; Gadonas, R. Bestimmung von Lebensdauern und Transienten absorptionsspektren von Polymethinfarbstoffen aus pikosekunden-spektroskopischen Messungen. *J. Signalaufzeichnungsmater.* **1984**, *12*, 319−328.
(28) Köhn, F.; Hofkens, J.; Wiesler, U.-M.; Cotlet, M.; van der Auweraer, M.; Müllen, K.; De Schryver, F. C. Single-molecule spectroscopy of a dendrimer-based host−guest system. *Chem.—Eur. J*. **2001**, *7*, 4126−4133.
(29) *Conn's Biological Stains*, 9th ed.; Lilie, R. D., Ed.; Williams and Wilkins: Baltimore, 1977; pp 252−253.
(30) Sabaté, R.; Esterlich, J. Aggregation characteristics of ovalbumin in β-sheet conformation determined by spectroscopy. *Biopolymers* **2002**, *67*, 113−120.
(31) Sabaté, R.; Esterlich, J. Pinacyanol as effective probe of fibrillar β-amyloid peptide: Comparative study with Congo Red. *Biopolymers* **2003**, *72*, 455−463.
(32) Voigt, B.; Nowak, F.; Ehlert, J.; Beenken, W. J. D.; Leupold, D.; Sandner, W. Substructures and different energy relaxation time within the first electronic transition of pinacyanol. *Chem. Phys. Lett*. **1997**, *278*, 380−390.
(33) Vompe, A. F.; Ivanova, L. V.; Meskhi, L. M.; Monich, N. V.; Raikhina, R. D. Reactions of polymethine dyes I. Synthesis of the pseudobases of polymethines dyes and their transformations. *Zh. Org. Khim.* **1985**, *21/3*, 584−594 (translation).
(34) Reichardt, C. Solvatochromic Dyes as Solvent Polarity Indicators. *Chem. Rev*. **1994**, *94*, 2319−2358.
(35) Militello, V.; Vetri, V.; Leone, M. Conformational changes involved in thermal aggregation processes of bovine serum albumin. *Biophys. Chem*. **2003**, *105*, 133−141.

JM050459+